Research Article

Chemical Review and Letters
journal homepage: www.chemrevlett.com
ISSN (online): 2645-4947 (print) 2676-7279

Kinetic and mechanistic insights into the atmospheric hydrogen abstraction of 3-hydroxybutanal by chlorine

Patouossa Issofa[1,*], Njabon Njankwa Eric[1], Tagne Tchamba Sédric[1], Emadak Alphonse[1]

[1]*Physical and Theoretical Chemistry Unit, Laboratory of Applied Physical and Analytical Chemistry, Faculty of Sciences, University of Yaoundé I, Yaoundé, Cameroon.*

ARTICLE INFO

Article history:
Received 03 July 2025
Received in revised form 01 September 2025
Accepted 11 October 2025

Keywords:
Atmospheric reaction
Reaction pathway
Vibrational frequencies
Transition state
Kinetics and thermodynamic parameters

ABSTRACT

This work investigates the reaction mechanism of hydrogen atom abstraction from 3-hydroxybutanal (3HB) by the chlorine (Cl) radical under atmospheric conditions, a process relevant to the degradation of volatile organic compounds (VOCs). Density Functional Theory (DFT) calculations were carried out at the B3LYP/def2-SVP level to explore five possible abstraction pathways, each involving a distinct hydrogen site within the 3HB molecule. Vibrational frequency analyses confirmed the presence of five corresponding transition states (TS_1–TS_5). Rate constants for each pathway were computed using KiSThelP software across a temperature range of 278–400 K. The calculated rate constants are 2.5817×10^{1}, 1.6695×10^{-7}, 8.3975×10^{2}, 1.1758×10^{-11}, and 2.3056×10^{-10} $cm^3 \cdot molecule^{-1} \cdot s^{-1}$ for pathways 1 through 5, respectively. These results indicate that hydrogen abstraction at site 3 (pathway 3) is the most kinetically favorable. Thermodynamic analysis supports this conclusion, with the product from pathway 3 exhibiting the lowest Gibbs free energy and reaction enthalpy (–22.25 kcal/mol), confirming it as the most thermodynamically stable. All pathways are exothermic and exergonic. These findings provide detailed mechanistic insight into the atmospheric reactivity of 3HB and may be extended to other structurally related VOCs, contributing to a better understanding of atmospheric oxidation processes

1. Introduction

Photolysis is among the most common chemical processes occurring in the atmosphere [1]. It involves the absorption of electromagnetic radiation, which typically initiates the breaking of chemical bonds and leads to the formation of highly reactive free radicals [2,3]. These radicals, which act as atmospheric oxidants, are of significant interest in atmospheric chemistry. Notable examples include the hydroxyl radical and the chlorine atom.

Hydroxyl radicals (OH) are often referred to as the "atmosphere's detergents" because of their high reactivity with a wide range of organic compounds [4], including ozone [5]. Ozone plays a critical role in photochemical smog formation and significantly affects the behavior of volatile organic compounds (VOCs)[4,6,7].

Chlorine atoms are especially prevalent in marine and coastal environments, where they are generated through multiphase reactions involving sea salt aerosols [8]. Although less abundant than hydroxyl or nitrate radicals, chlorine atoms exhibit exceptionally high reactivity [9-11]. This makes the oxidation of VOCs by chlorine a topic of considerable interest. The resulting organic products can be efficiently removed from the atmosphere via absorption, biodegradation, or further chemical reactions.

Numerous theoretical and experimental studies have investigated the atmospheric reactions of VOCs with hydroxyl radicals and chlorine atoms [12]. However, little research has focused on the reactivity of these oxidants with hydroxy-carbonyl compounds, despite their significant role in air quality degradation [13]. Only a limited number of hydroxy-ketones have been studied in this context [14-18], and for hydroxy-aldehydes, existing literature primarily addresses their reaction kinetics with hydroxyl radicals [19,20].

In this work, we explore the reaction mechanism of 3-hydroxybutanal (3HB) with chlorine atoms under atmospheric conditions. To our knowledge, no previous

* Corresponding author E-mail: patouossa12@yahoo.fr
https://doi.org/10.22034/crl.2025.532470.1648
This work is licensed under Creative Commons license CC-BY 4.0

study has examined the kinetics and thermodynamics of hydrogen abstraction from 3HB by chlorine atoms.

Hydrogen abstraction in 3HB can occur at five different sites—CHO(1), CH_2(2), CHOH(3), CH_3(4), and OH(5)—resulting in five potential reaction pathways, as illustrated in Scheme 1.

2. Materials and Methods

Reactants, intermediates, transition states, and products were fully optimized using the B3LYP hybrid functional combined with the def2-SVP basis set, as implemented in the ORCA 4.2.1 software [21]. This level of theory (B3LYP/def2-SVP) has been demonstrated to yield reliable insights into reaction mechanisms [22–24]. Transition states were identified through the 'Relaxed Surface Scan' method. The presence of a single imaginary frequency, along with its animated mode and intrinsic reaction coordinate (IRC) calculations, confirmed the connection between each transition state and its corresponding reactants and products. Vibrational frequency analyses verified that the predicted stationary points are true minima on the potential energy surface.

Thermodynamic parameters including internal energy, enthalpy, and Gibbs free energy for all species involved (reactants, intermediates, transition states, and products) were calculated under standard temperature and pressure conditions using equations (1) to (3). The overall enthalpy and Gibbs free energy [25,26] changes for the reaction were determined using equations (4) and (5), respectively.

$$U = E(el) + E(ZPE) + E(vib) + E(rot) + E(trans) \quad (1)$$

$$H = U + k_B T \quad (2)$$

$$G = H - TS \quad (3)$$

$$\Delta_r H = \sum H(products) - \sum H(reactants) \quad (4)$$

$$\Delta_r G = \sum G(products) - \sum G(reactants) \quad (5)$$

Equation (6) was used to calculate the bond dissociation enthalpy (BDE).

$$BDE = H(3HB^{\bullet}) + H(H^{\bullet}) - H(3HB - H) \quad (6)$$

The rate constants for the elementary reactions were computed using the KiSThelP software (version 2002) [27], a multiplatform program. Transition state theory was applied to determine the parameters A and E_a in the Arrhenius equation for the rate constant k [26], as shown in Equation (7).

$$k = Ae^{-E_a/RT} \quad (7)$$

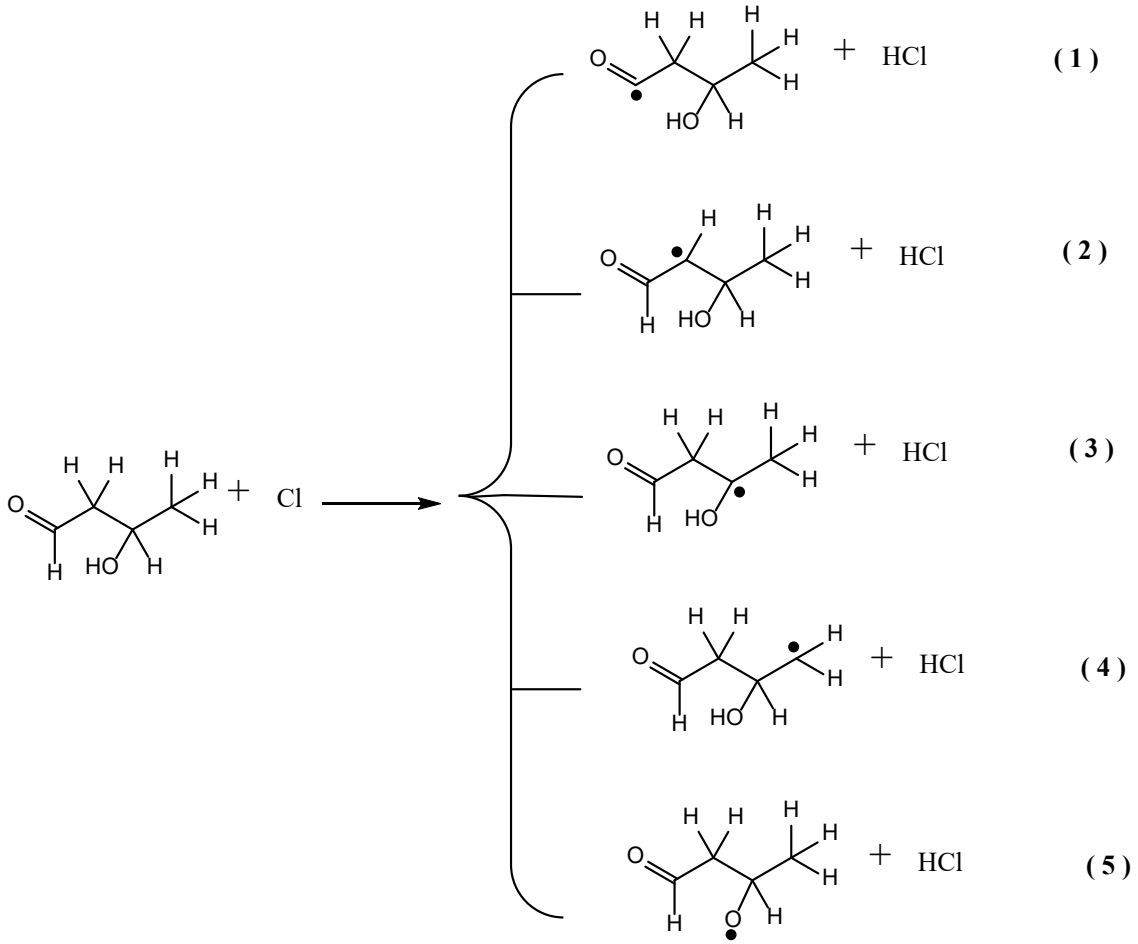

Scheme 1. Different possible reaction pathways between 3HB and Cl.

3. Results and Discussion

3.1. Structure optimization

The hydrogen abstraction reaction on 3HB occurs in two stages. First, the chlorine radical approaches the 3HB molecule, forming an intermediate complex that is more stable than the initial reactants. In the second stage, this intermediate complex dissociates into the reaction products after overcoming an energy barrier corresponding to a transition state. This stepwise, uncoordinated mechanism is outlined below.

$$3HB + {}^{\bullet}Cl \longrightarrow \text{Intermediate Complex } (\mathbf{I}) \xrightarrow{TS} \text{Product}(\mathbf{P})$$

Scheme 2. Reaction mechanism

Figure 1 presents the optimized structure of 3HB, displaying the bond distances between atoms in angstroms (Å) as determined through optimization. The values in parentheses represent the corresponding experimental measurements. Figure 2 presents the structures of five (05) reaction intermediates labeled I_1, I_2, I_3, I_4, and I_5 formed through the approach of a Cl radical to compound 3HB, specifically near the hydrogen atom targeted for abstraction.

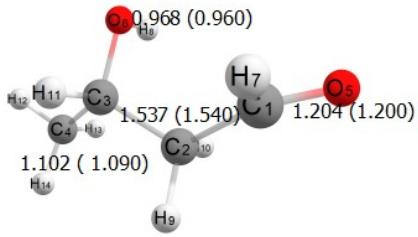

Fig. 1. Optimized structure of 3HB

The C–H bond distances involved in the reaction for intermediates I_1 through I_5 are 1.246, 1.171, 1.307, and 1.135 Å, respectively. For intermediate I_5, the O–H bond length is 0.983 Å. Additionally, the H–Cl bond distances in I_1, I_2, I_3, I_4, and I_5 are 1.669, 1.781, 1.585, 1.899, and 2.000 Å, respectively. Figure 3 illustrates the various possible transition states of the reaction: TS_1 (hydrogen abstraction from the CHO group), TS_2 (from the $–CH_2–$ group), TS_3 (from the –CH– group), TS_4 (from the $–CH_3$ group), and TS5 (from the –OH group). These transition states correspond to the formation of products P_1 through P_5, respectively. Each is characterized by a nearly linear alignment of the chlorine atom with the abstracted hydrogen and the central atom involved in the abstraction.

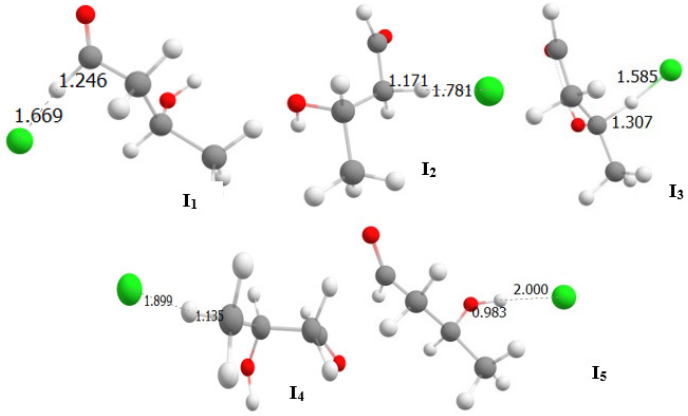

Fig. 2. Optimized structure of reaction intermediates denoted I_1, I_2, I_3, I_4 and I_5

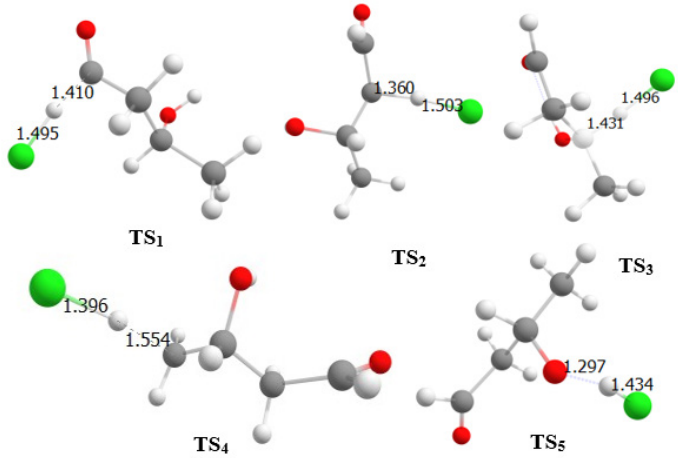

Fig. 3. Optimized structure of transition state TS_1, TS_2, TS_3, TS_4 and TS_5.

The calculation of vibrational frequencies for the transition states reveals the presence of a single imaginary frequency for each, with the following values: -396.93 cm^{-1} for TS_1, 916.37 cm^{-1} for TS_2, -341.07 cm^{-1} for TS_3, -361.63 cm^{-1} for TS4, and -704.04 cm^{-1} for TS_5. The C–H and O–H bond lengths in the various transition states range from 1.297 Å to 1.554 Å. The corresponding H–Cl bond lengths are 1.495 Å (TS_1), 1.503 Å (TS_2), 1.496 Å (TS_3), 1.397 Å (TS_4), and 1.434 Å (TS_5).

As the chlorine radical (•Cl) approaches the hydrogen atom to be abstracted, the C–H (or O–H in TS_5) bond length increases, while the H–Cl distance decreases. This behavior is attributed to the high electronegativity of chlorine, which strongly attracts the hydrogen's electron.

The products P_1 through P_5, formed via intermediates I_1 to I_5 and transition states TS_1 to TS_5, are depicted in Figure 4. Among them, product P_3, which forms a six-membered ring, appears to be the most stable.

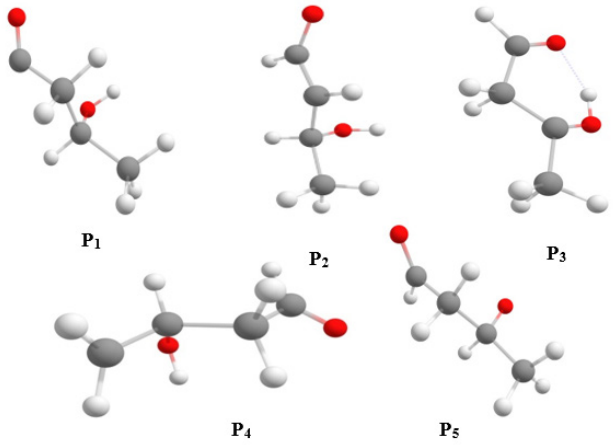

Fig. 4. Optimized structure of products P_1, P_2, P_3, P_4 and P_5.

The relative enthalpies and Gibbs free energies of the various species involved in the reaction pathways were calculated at the B3LYP/def2-SVP level of theory under standard temperature and pressure conditions. All values are reported in kcal/mol, as summarized in Table 1. The transition states (TS) associated with the hydrogen abstraction pathways in the reaction of 3-hydroxybutanal (3HB) with a chlorine atom exhibit negative energy barriers, indicating highly favorable transitions. The computed energy barriers follow the order: TS_3 (–25.79 kcal/mol) < TS_1 (–23.42 kcal/mol) < TS_2 (–12.50 kcal/mol) < TS_5 (–8.73 kcal/mol) < TS_4 (–6.31 kcal/mol), clearly identifying pathway 3 as the most kinetically favorable route.

The reaction enthalpies (ΔrH) for the formation of products P_1 through P_5 are –18.68, –21.11, –22.25, –2.58, and –5.98 kcal/mol, respectively. These values confirm the exothermic nature of all five pathways. Among them, product P_3 is the most thermodynamically stable, with the lowest relative enthalpy (–22.25 kcal/mol).

These results are in agreement with previous findings by Messaadia et al. [14] and Sleiman et al. [18], who observed a similar preference for hydrogen abstraction at the β-position in reactions involving OH radicals. The enhanced reactivity at this site is attributed to its favorable activation profile, both kinetically and thermodynamically.

Table 1. Relative enthalpy (ΔrH) and Gibbs energy (ΔrG) of the different states 3HB reacting with Cl

Different states of 3HB + Cl	Δ_rH(kcal/mol)	Δ_rG(kcal/mol)
3HB + Cl	0.00	0.00
I_1	-18.67	-22.52
I_2	-6.74	-11.28
I_3	-22.30	-26.42
I_4	-4.16	-9.19
I_5	-10.92	-19.18
TS_1	-18.24	-23.42
TS_2	-8.88	-12.50
TS_3	-21.59	-25.79
TS_4	-2.47	-6.31
TS_5	-5.34	-8.73
P_1+ HCl	-18.68	-27.85
P_2+ HCl	-21.11	-25.42
P_3+ HCl	-22.25	-30.74
P_4+ HCl	-2.58	-7.38
P_5+ HCl	-5.98	-10.59

Table 2 presents the bond dissociation enthalpy (BDE) values for the various hydrogen abstraction sites in 3HB. BDE serves as a reliable indicator of bond strength lower BDE values correspond to weaker bonds that are more easily broken, whereas higher values indicate stronger, more stable bonds [11].

Table 2. Bond dissociation enthalpies (BDE) of the different hydrogen abstraction sites of the 3-hydroxybutanal compound

Liaison	BDE (kcal/mol)
C_1-H (Site 1)	85.85
C_2-H (Site 2)	86.79
C_3-H (Site 3)	82.83
C_4-H (Site 4)	98.68
O-H (Site 5)	98.67

The C_3–H bond at site (3) exhibits the lowest BDE value (82.83 kcal/mol), indicating that it is the most susceptible to cleavage, as shown in Table 3. In contrast, the C_4–H bond at site (4) has the highest BDE (98.68 kcal/mol), making it the most resistant to bond breaking. These results are consistent with both thermodynamic and kinetic analyses.

Figure 5 illustrates the IRC trajectory for the reaction between 3HB and the •Cl radical, showing a connection between reactants and products via an intermediate and a transition state (TS), regardless of the abstraction site.

The analysis of Figure 5 confirms that the products are formed at a lower energy level than the reactants, with negative energy barriers. This indicates that the reaction between 3-hydroxybutanal and chlorine is predominantly

exothermic and exergonic, consistent with findings by Rouichi et al. [12]. Hydrogen abstraction at site (3), corresponding to the –CH group bearing the hydroxyl function, is the most favorable pathway and yields the highest product formation. This is due to its lower energy barrier and the smallest reaction enthalpy. Conversely, hydrogen abstraction at site (4), which has the highest energy barrier, is the least favorable and contributes minimally to product formation.

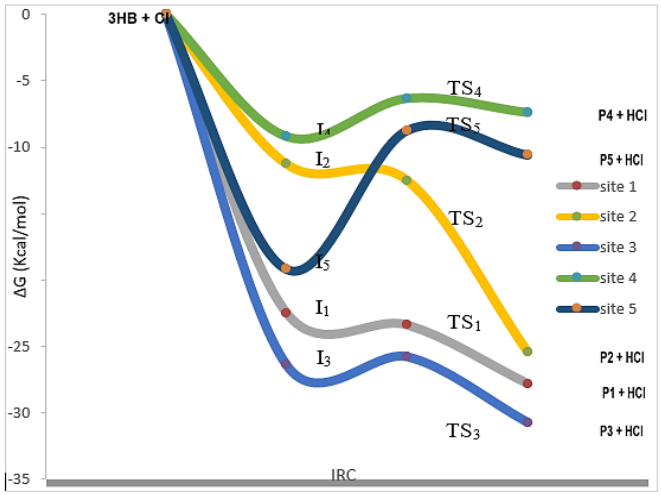

Fig. 5. H-abstraction profile of 3HB reaction with Cl

3.2. Kinetic study

The reaction of 3-hydroxybutanal (3HB) with a chlorine atom involves competition between five possible hydrogen abstraction pathways, corresponding to five distinct sites, as illustrated in the mechanism below:

$$3HB + Cl \xrightarrow{k_1} P_1 + HCl \quad \text{path 1}$$

$$\xrightarrow{k_2} P_2 + HCl \quad \text{path 2}$$

$$\xrightarrow{k_3} P_3 + HCl \quad \text{path 3}$$

$$\xrightarrow{k_4} P_4 + HCl \quad \text{path 4}$$

$$\xrightarrow{k_5} P_5 + HCl \quad \text{path 5}$$

Scheme 3. H-abstraction paths

Rate constants k_1, k_2, k_3, k_4, and k_5 correspond to pathways 1 through 5, respectively (see Scheme 3: H-abstraction paths).

The rate constants for each pathway were calculated using the KiSThelP software. Simulations were conducted at a pressure of 1 atm and across a temperature range of 278 to 400 K. A scaling factor of 0.89 was applied to the vibrational frequencies previously obtained via DFT calculations. All reported rate constants are given in units of $cm^3 \cdot molecule^{-1} \cdot s^{-1}$, with temperatures expressed in Kelvin (K).

Temperature significantly influences this reaction. At room temperature (298 K), the calculated rate constants are as follows (in $cm^3 \cdot molecule^{-1} \cdot s^{-1}$):

- Pathway 1: 2.5817×10^{1}
- Pathway 2: 1.6695×10^{-7}
- Pathway 3: 8.3975×10^{2}
- Pathway 4: 1.1758×10^{-11}
- Pathway 5: 2.3056×10^{-10}

These results show that the hydrogen abstraction at site 3, corresponding to the carbon atom bonded to the hydroxyl group (via TS_3), is the most favorable pathway, with the highest rate constant (8.3975×10^{2} $cm^3 \cdot molecule^{-1} \cdot s^{-1}$), indicating a relatively fast reaction. In contrast, abstraction at site 4, with the lowest rate constant (1.1758×10^{-11} $cm^3 \cdot molecule^{-1} \cdot s^{-1}$), represents the slowest reaction pathway.

4. Conclusion

In conclusion, the DFT-based kinetic and mechanistic study of hydrogen abstraction from 3-hydroxybutanal (3HB) by chlorine atoms demonstrates that all reaction pathways are exothermic and exergonic. Pathway 3, involving hydrogen abstraction at site 3, emerges as the most favorable route due to its lowest energy barrier and the formation of the most stable product, a finding further supported by its highest rate constant. These insights contribute to a deeper understanding of 3HB reactivity and can be applied to similar volatile organic compounds, aiding the refinement of atmospheric chemistry models and environmental protection strategies.

References

[1] G. S. James, Reaction mechanisms in environmental engineering, Butterworth-Heineman, Oxford, United Kingdom (2018).

[2] Y. Zhang, B. He and Y. Sun, Computational study on mechanisms and kinetics of the atmospheric $\text{CFCl}_2\text{CH}_2\text{O}_2$ with Cl reaction. *J. Mol. Graph. Model.*, 99 (2020) 107618.

[3] B. Çalişkan and A. C. Çalişkan, Interaction with matter of ionizing radiation and radiation Damages (Radicals), InTech (2018).

[4] R. Atkinson, D. L. Baulch, R. A. Cox, J. N. Crowley, R. F. Hampson, R. G. Hynes et al., Evaluated kinetic and photochemical data for atmospheric chemistry: Gas phase reactions of organic species. *Atmos. Chem. Phys.*, 6 (2006) 3625-4055.

[5] E. F. Danielsen, Stratosphere-troposphere exchange based on radioactivity, ozone and potential vorticity. *J. Atmos. Sci.*, 25 (1968) 502-518.

[6] R. Delmas, G. Mégie and V. H. Peuch, Physique et chimie de l'atmosphère, Belin, Paris (2005).

[7] J. D. Fenske, A. S. Hasson, S. E. Paulson, K. T. Kuwata, A. Ho and K. N. Houk, The pressure dependence of the OH radical yield from ozone-alkene reactions. *J. Phys. Chem. A*, 104 (2000) 7821-7833.

[8] A. P. Pszenny, E. V. Fischer, R. S. Russo, B. C. Sive, R. K. Varner and A. White, Estimates of Cl atom concentrations and hydrocarbon kinetic reactivity in surface air at Appledore island. Maine (USA) during ICARTT CHAIOS. *J. Geophys. Res.*, 112 (2007).

[9] C. Chang-Tang, L. Tsun-Hsien and J. Fu-Tien, Atmospheric concentrations of the Cl atom, CIO radical, and HO radical in the coastal marine boundary layer. *Environ. Res.*, 94 (2004) 67-74.

[10] O. V. Rattigan, H. W. Sidebottom, J. J. Treacy and O. J. Nielsen, The Reaction of hydroxyl radicals and chlorine atoms with sulphur dioxide. *Proc. R. Ir. Acad., B*, 89 (1989) 353–361.

[11] C. B. Faxon and D. T. Allen, Chlorine chemistry in urban atmospheres: a review. *Environ. Chem.*, 10 (2013) 221-233.

[12] R. Koppmann, Chemistry of volatile organic compounds in the atmosphere. In: Wilkes, H. (eds) Hydrocarbons, Oils and Lipids: Diversity, Origin, Chemistry and Fate. Handbook of Hydrocarbon and Lipid Microbiology, Springer, Cham (2020).

[13] S. Lelieveld, J. Wilson, E. Dovrou, A. Mishra, P. S. J. Lakey, M. Shiraiwa et al., Hydroxyl radical production by air pollutants in epithelial lining fluid governed by interconversion and scavenging of reactive oxygen species. *Environ. Sci. Technol.*, 55 (2021) 14069-14079.

[14] L. Messaadia, G. El Dib, M. Lendar, M. Cazaunau, E. Roth, A. Ferhati et al., Gas-phase rate coefficients for the reaction of 3-hydroxy-2-butanone and 4-hydroxy-2-butanone with OH and Cl. *Atmos. Environ.*, 77 (2013) 951-958.

[15] R. Cheramangalath Balan and B. Rajakumar, Photo-Oxidation reaction kinetics and mechanistics of 4-Hydroxy-2-butanone with Cl atoms and OH radicals in the gas Phase. *J. Phys. Chem. A*, 123 (2019) 4342−4353.

[16] S. Rouichi, S. Samai, A. Ferhati and A. Chakir, Atmospheric Reaction of Cl with 4-Hydroxy-2-pentanone (4H2P): A Theoretical Study. *J. Phys. Chem. A*, 122 (2018) 2135−2143.

[17] R. Cheramangalath Balan and B. Rajakumar, Photo-Oxidation Reaction Kinetics and Mechanistics of 4-Hydroxy-2-butanone with Cl Atoms and OH Radicals in the Gas Phase. *J. Phys. Chem. A*, 123 (2019) 4342−4353.

[18] C. Sleiman, G. El Dib, B. Ballesteros, A. Moreno, J. Albaladejo, A. Canosa et al., Kinetics and Mechanism of the Tropospheric Reaction of 3-Hydroxy-3-Methyl-2-Butanone With Cl Atoms. *J. Phys. Chem. A*, 118 (2014) 6163-6170.

[19] M. Blanco, I. Barnes and P. Wiesen, Kinetic Investigation of the OH Radical and Cl Atom Initiated Degradation of Unsaturated Ketones at Atmospheric Pressure and 298 K. *J. Phys. Chem. A*, 116 (2012) 6033-6040.

[20] J. A. Kerr and D. W. Sheppard, Kinetics of the reactions of hydroxyl radicals with aldehydes studied under atmospheric conditions. *Environ. Sci. Technol.*, 15 (1981) 960-963.

[21] F. Neese, The ORCA program system. *Wiley Interdiscip. Rev. Comput. Mol. Sci.*, 2 (2012) 73-78.

[22] A. Collado, M. Gómez-Gallego, A. Santiago and M. A. Sierra, Understanding the reactivity of group 6 Metal (M= Cr, W) alkynyl fischer carbene complexes with multiReactive masked dienes. *Eur. J. Org. Chem.*, 2 (2019) 369-377.

[23] J. Tirado-Rives and W. L. Jorgensen, Performance of B3LYP density functional methods for a large set of organic molecules. *J. Chem. Theory Comput.*, 4 (2008) 297-306.

[24] N. Nasehi, B. Mirza and S. Soleimani-Amiri, Experimental and theoretical investigation on imidazole derivatives using magnetic nanocatalyst: green synthesis, characterization, and mechanism study. *Polycyclic Aromat. Compd.*, 43 (2023) 7890-7911.

[25] J. N. Nouping Fekoua, I. Patouossa, E. N. Njabon, J. F. Kenmogne Tchidjo, E. Kamseu, G. Bebga et al., Computational study on the Al^{3+} substitution and porous agent effect on geopolymer foam formation. *Chem. Rev. Lett.*, 7 (2024) 142–147.

[26] I. Patouossa Issofa, E. N. Njabon, G. C. Kapche Simo, J. U. Badoana Boyomo and A. Emadak, Theoretical mechanistic and kinetic study on the [1, 5]-H shift in (z)-hexa-1,3-diene. *Chem. Res. Tech.*, 1 (2024) 89-94.

[27] S. Canneaux, F. Bohr and E. Henon, KiSThelP: a program to predict thermodynamic properties and rate constants from quantum chemistry results. *J. Comput. Chem.*, 35 (2014) 82-93.